JOURNAL OF MAGNETIC RESONANCE **18**, 69–83 (1975)

NMR Fourier Zeugmatography

ANIL KUMAR, DIETER WELTI, AND RICHARD R. ERNST

Laboratorium für Physikalische Chemie, Eidgenössische Technische Hochschule, 8006 Zürich, Switzerland

Received August 2, 1974

A new technique of forming two- or three-dimensional images of a macroscopic sample by means of NMR is described. It is based on the application of a sequence of pulsed magnetic field gradients during a series of free induction decays. The image formation can be achieved by a straightforward two- or three-dimensional Fourier transformation. The method has the advantage of high sensitivity combined with experimental and computational simplicity.

I. INTRODUCTION

P. C. Lauterbur (*1*) has recently described an ingenious technique to determine one-, two- or three-dimensional images of the distribution of magnetic moments in a macroscopic sample. He calls such an image a zeugmatogram. The potential use of this method includes the measurement of the spatial distribution of a given nuclear species in living tissue and the determination of its relaxation times with the possibility of localizing cancerous parts in a living organism (*2*, *3*). The most important nuclei to be detected are the protons of water in biological materials.

Lauterbur's method (*1*) is based on the application of linear magnetic field gradients in different directions in a series of experiments. Each of the resulting spectra of a single resonance line represents a distribution function of the nuclei as a function of the local magnetic field strength. It can be considered as a projection of the three-dimensional nuclear spin density onto the axis along which the linear field gradient has been applied. From a sufficient number of such projections onto different axes, it is possible to partially reconstruct the two- or three-dimensional spin density function by means of well-known image reconstruction techniques (*4–7*). The inherent spatial resolution is determined by the number of independent projections obtained and by the natural width of the resonance line under consideration. The various linear gradients along different directions can be generated either by means of a set of suitable gradient coils or, more easily, by means of a single gradient coil and step-by-step rotation of the sample.

A modification of the Lauterbur technique (*1*) can be obtained by the application of Fourier spectroscopy techniques (*8*). For each gradient setting, a free induction decay signal (FID) is recorded. Except for improved sensitivity and for the elimination of one computational step (many image reconstruction techniques require as an intermediate step the Fourier transformation of the spectrum (*4*, *7*)), this method does not show advantages over the Lauterbur procedure and it will not be mentioned further.

DOI of original item: doi: 10.1016/0022-2364(75)90224-3

In this paper, an alternative technique is described which is remarkable for its experimental and computational simplicity and by its inherent high sensitivity. It is based on the application of a sequence of pulsed orthogonal linear field gradients to the sample during the FID. The spatial spin density function can then be reconstructed by a straightforward two- or three-dimensional Fourier transformation. One of the important features of this method is the homogenous error distribution over the entire frequency range such that low and high frequency components can be reconstructed with equal accuracy. The method can easily be implemented on a small on-line computer.

II. MATHEMATICAL ANALYSIS OF THE TECHNIQUE

Although the experimental examples presented in this paper and probably many of the future applications of this technique will be confined to the two-dimensional imaging of a sample, the theory will be developed for the more general three-dimensional case.

The principle of the technique is explained by means of Fig. 1. At time $t = 0$, an FID is generated by means of a short 90° pulse. In the course of this decay, three orthogonal

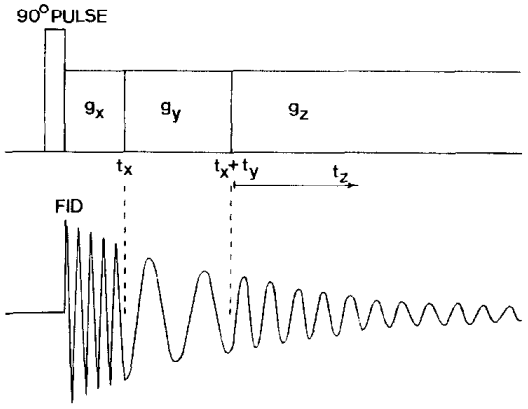

FIG. 1. Diagram depicting the principle of the zeugmatographic method. The FID is recorded during the third time-interval as a function of t_z. For a three-dimensional zeugmatogram, usually N^2 such FID signals will be needed for a complete set of values for x- and y-gradients. N is the number of samples in an FID.

linear magnetic field gradients, g_x, g_y, and g_z, are applied in succession. The z-component of the local magnetic field is then given by

$$H_z(\mathbf{r}) \begin{cases} = H_0 + g_x x, & \text{for} \quad 0 < t < t_x \\ = H_0 + g_y y, & \text{for} \quad t_x < t < t_x + t_y \\ = H_0 + g_z z, & \text{for} \quad t_x + t_y < t. \end{cases} \qquad [1]$$

The FID is sampled in the third time-interval as a function of $t_z = t - (t_x + t_y)$. It is at the same time a function of the preceding time-intervals t_x and t_y. It will be denoted by $s(\mathbf{t}) = s(t_x, t_y, t_z)$. The experiment is repeated for a full set of equally spaced t_x and t_y values. It will be shown in this section that the three-dimensional Fourier transform of $s(\mathbf{t})$ is a measure for the spatial spin density function $c(\mathbf{r}) = c(x,y,z)$ and provides a three-dimensional image of the sample.

The observed signal $s(\mathbf{t})$ is a composite of the contributions from the various volume elements of the sample and can be written as

$$s(\mathbf{t}) = \iiint c(\mathbf{r})\, s(\mathbf{r},\mathbf{t})\, dv \qquad [2]$$

where $s(\mathbf{r},\mathbf{t})\, dv$ is the contribution from the volume element $dv = dx\, dy\, dz$ at position $\mathbf{r}$. For a single resonance, the function $s(\mathbf{r},\mathbf{t})$ can easily be found by solving Bloch equations. After phase-sensitive detection with the frequency ω_1, the signal is given by

$$s(\mathbf{r},\mathbf{t}) = M_0 \cos\{(\Delta + \eta_x x)t_x + (\Delta + \eta_y y)t_y + (\Delta + \eta_z z)t_z\} \cdot \exp\{-(t_x + t_y + t_z)/T_2\}. \qquad [3]$$

The resonance offset in the absence of a field gradient is given by $\Delta = -\gamma H_0 - \omega_1$. The field gradients $\eta_k = -\gamma g_k$ are measured in frequency units. The setting of the phase-sensitive detector has been assumed arbitrarily to produce a cosine signal. It can easily be shown that the function $|\bar{c}(\mathbf{r})|$, which is plotted in a Fourier zeugmatogram, is independent of this arbitrary phase setting.

The three-dimensional Fourier transform of $s(\mathbf{t})$ is denoted by $S(\boldsymbol{\omega}) = S(\omega_x,\omega_y,\omega_z)$ and is given by

$$S(\boldsymbol{\omega}) = \iiint s(\mathbf{t}) \exp(-i\boldsymbol{\omega}\mathbf{t})\, dt_x\, dt_y\, dt_z. \qquad [4]$$

It is again a composite of the contributions from the various volume elements,

$$S(\boldsymbol{\omega}) = \iiint c(\mathbf{r})\, S(\mathbf{r},\boldsymbol{\omega})\, dv. \qquad [5]$$

Here, $S(\mathbf{r},\boldsymbol{\omega})$ is the Fourier transform of $s(\mathbf{r},\mathbf{t})$ and is calculated to be

$$\begin{aligned} S(\mathbf{r},\boldsymbol{\omega}) = \tfrac{1}{2}\{&G(\Delta + \eta_x x - \omega_x)\, G(\Delta + \eta_y y - \omega_y)\, G(\Delta + \eta_z z - \omega_z) \\ &+ G(-\Delta - \eta_x x - \omega_x)\, G(-\Delta - \eta_y y - \omega_y)\, G(-\Delta - \eta_z z - \omega_z)\} \end{aligned} \qquad [6]$$

with the complex line shape function

$$G(\omega) = A(\omega) + iD(\omega) = \frac{M_0/T_2}{(1/T_2)^2 + \omega^2} + i\frac{M_0\omega}{(1/T_2)^2 + \omega^2}. \qquad [7]$$

The second term in Eq. [6] which describes the contribution of the resonance near $-\Delta$ can be neglected whenever the linewidth is small compared to Δ.

Equation [6] shows that the following identity holds,

$$S(\mathbf{r},\boldsymbol{\omega}) = S(\mathbf{0},\boldsymbol{\omega} - \eta\mathbf{r}) \qquad [8]$$

where η is a diagonal matrix with the elements η_x, η_y, and η_z. One obtains for $S(\boldsymbol{\omega})$

$$S(\boldsymbol{\omega}) = \iiint c(\mathbf{r})\, S(\mathbf{0},\boldsymbol{\omega} - \eta\mathbf{r})\, dv. \qquad [9]$$

The frequency variable $\boldsymbol{\omega}$ will now be replaced by a spatial variable $\mathbf{r}'$ with

$$\boldsymbol{\omega} = \Delta\mathbf{I} + \eta\mathbf{r}'. \qquad [10]$$

$\mathbf{I}$ is the vector (1, 1, 1). Then, one obtains

$$S(\boldsymbol{\omega}) = S(\Delta\mathbf{I} + \eta\mathbf{r}') = \bar{c}(\mathbf{r}') = \iiint c(\mathbf{r})\, S(\mathbf{0}, \Delta\mathbf{I} + \eta(\mathbf{r}' - \mathbf{r}))\, dv. \qquad [11]$$

This integral is clearly a three-dimensional convolution integral. It represents a "filtered" spin density function $\bar{c}(\mathbf{r}')$ obtained from the original spin density function $c(\mathbf{r})$ by a convolution with the lineshape function $S(\mathbf{0}, \Delta\mathbf{I} + \eta\mathbf{r})$. By means of Eq. [6] and neglecting the contribution of the resonance near $-\Delta$, one obtains finally

$$\bar{c}(\mathbf{r}') = \tfrac{1}{2}\iiint c(\mathbf{r})\, G(\eta_x(x - x'))\, G(\eta_y(y - y'))\, G(\eta_z(z - z'))\, dv. \qquad [12]$$

The filtered spin density function $\bar{c}(\mathbf{r}')$ is a complex function. Its real and its imaginary parts both contain products of absorption- and dispersion-like parts and can have positive and negative function values. It is, therefore, advisable to compute and plot the absolute value $|\bar{c}(\mathbf{r}')|$ rather than plotting $\mathrm{Re}\{\bar{c}(\mathbf{r}')\}$ or $\mathrm{Im}\{\bar{c}(\mathbf{r}')\}$. For a sufficiently narrow resonance line or for sufficiently strong gradients η_x, η_y, and η_z, $|\bar{c}(\mathbf{r}')|$ is a good measure for $c(\mathbf{r}')$ itself. In Section IV, a modified technique is described that permits complete separation of absorption and dispersion mode signals.

In principle, it is also possible to utilize a quadrature phase detector that produces at its output $s(\mathbf{t})$ as well as the quadrature component $s'(\mathbf{t})$ which is given by equations similar to Eqs. [2] and [3] where the cosine function is replaced by a sine function. A linear combination of the two signals permits complete elimination of the contributions of the resonance near $-\Delta$. But the absorption and dispersion parts are not separated and the final result is equivalent to Eq. [12] except for an improvement of the sensitivity by a factor $\sqrt{2}$.

It is a major feature of the described technique that it does not involve one-dimensional projections of the three-dimensional spin density and that the Fourier transform of the spin density is directly measurable (except for the filtering caused by the natural lineshape of the NMR signal). Many of the image reconstruction techniques which can be used for the Lauterbur procedure (*1*) utilize the fact that the Fourier transform of a one-dimensional projection of the spin density represents a one-dimensional cross section of the three-dimensional Fourier transform of the spin density function (*7*). All the cross sections that can be obtained in this way pass through the point $\boldsymbol{\omega} = \mathbf{0}$. The density of the obtained samples, therefore, is maximum for $\boldsymbol{\omega} = \mathbf{0}$ and decreases for increasing $|\omega|$. To obtain equally spaced samples representing the Fourier transform, it is at first necessary to go through an interpolation procedure. This is a prerequisite for the execution of the inverse Fourier transformation that produces the desired image. This ultimately implies that the low frequency components are obtained with higher precision than the high frequency components of the zeugmatogram. Therefore, the coarse features are better represented than the details. In some cases, this may be no disadvantage, and it may, in particular cases, even be desirable. This feature is inherent and is independent of the reconstruction procedure used. It also occurs in direct algebraic reconstruction techniques (*6*) that do not involve a Fourier transformation.

In the described Fourier technique, on the other hand, an equal sample spacing of the Fourier transform is automatically obtained. The error distribution of a Fourier zeugmatogram is therefore homogenous over the spatial and over the covered frequency range, in contrast to the Lauterbur procedure. Coarse features and details are obtained with the same accuracy.

III. EXPERIMENTAL PROCEDURE AND RESULTS

The predominant problem in practical applications of Fourier zeugmatography is the economy of data storage. Three-dimensional zeugmatograms can be obtained in exceptional cases only because of the enormous amount of data required. Therefore, only the two-dimensional case will be discussed.

The experiments to be described in this section have been performed with standard equipment available in our laboratory. It has not been optimized for this particular purpose and could be improved in many respects. The set-up is indicated in Fig. 2. It

consists of a Varian high resolution 15-in. electromagnet with an 11-gradient shim system, a Bruker SXP4-100 high power pulse spectrometer with a Bruker single coil probe assembly for high power pulse experiments, and a Varian 620/L-100 computer system equipped with 12 k memory, a fast 12-bit analog-to-digital converter and a number of execute lines for the connection to the spectrometer.

The linear magnetic field gradients have been generated by means of the x- and z-gradient shim coils of the Varian shim system. The currents necessary to produce the linear field gradients have been generated by a set of external stable power supplies and

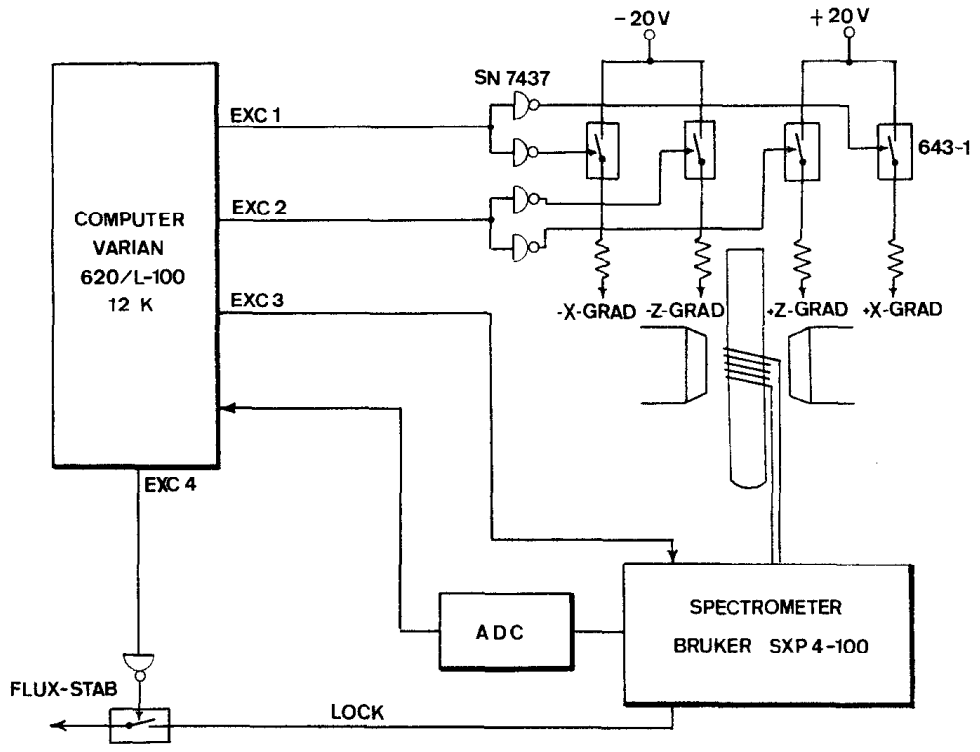

FIG. 2. Block diagram of the experimental set-up.

are computer-controlled by means of a series of very fast solid state DIP relays (Teledyne Relays 643-1) with a response time of less than 10 μsec. Currents of approximately 70 mA are necessary to generate field gradients of 1,000 Hz/cm.

The magnetic field has been stabilized by a Bruker B-SN 15 external pulsed proton lock with a long term stability of 1 Hz. To prevent a disturbance of the lock by the applied field gradients, it was necessary to interrupt the control loop during the application of the field gradients for approximately 100 msec. This did not affect the field stability.

The maximum number of samples representing the zeugmatogram is limited by the available memory size of the computer. In general, a quadratic image with $N \times N$ samples is desired. It is then necessary to record $2N$ FID's and to digitize each FID into $2N$ samples. To permit the use of a fast Fourier transform routine, N is usually selected to be a power of two.

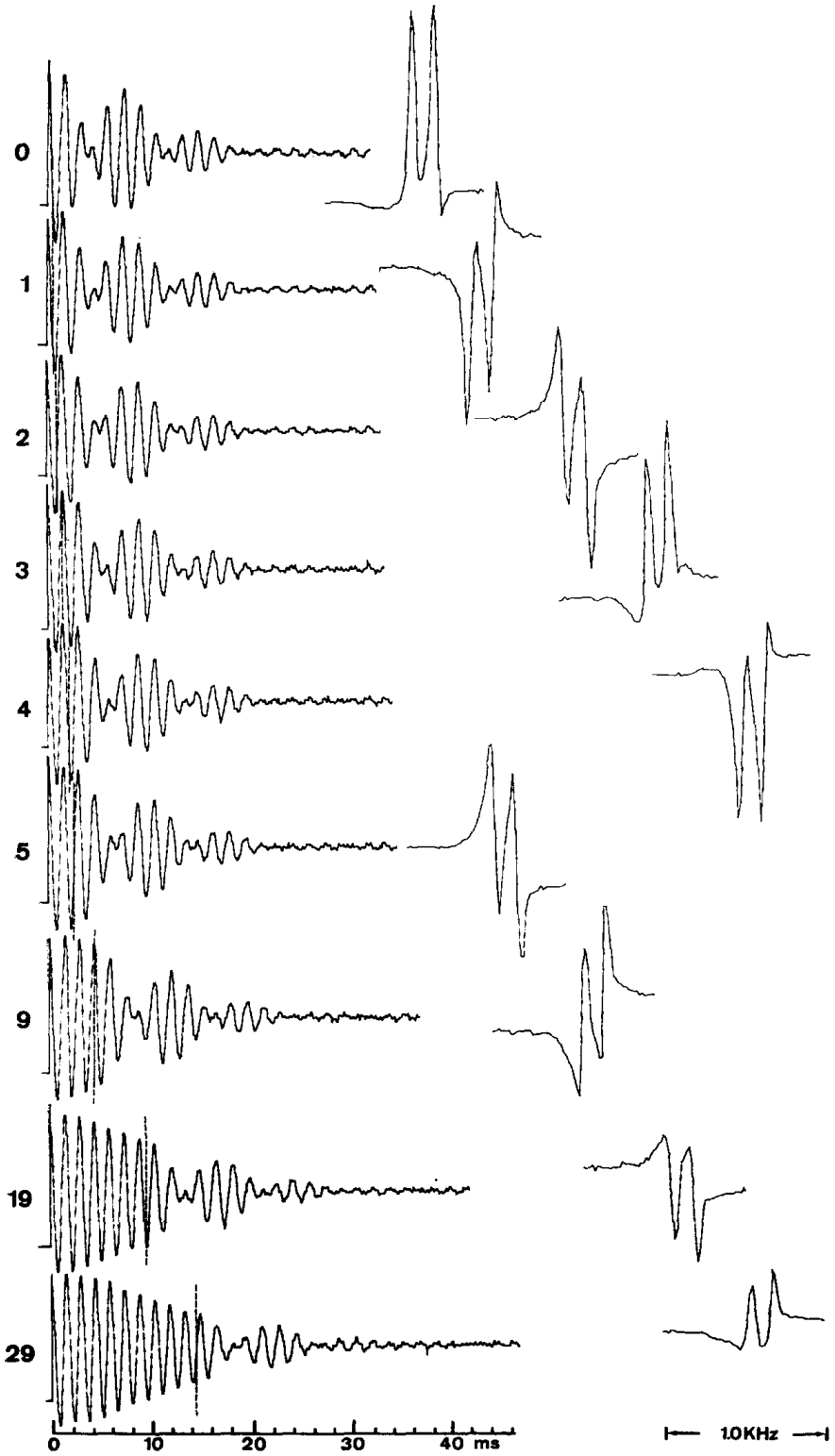

FIG. 3.

A well-known procedure to obtain a finer representation of a Fourier transform is the addition of a set of zeros to the array to be transformed (*9*). A simple method that requires only $N(N+2)$ memory locations but produces an $N \times N$ zeugmatogram is the following one. N FID's consisting of N samples each are recorded. To perform the first Fourier transformation, the N samples representing the FID k, $\{s_{k0}, s_{k1}, \ldots, s_{kN-1}\}$, are transferred to a separate memory block and are augmented by N zero values, $\{s_{k0}, s_{k1}, \ldots, s_{kN-1}, 0, 0, \ldots, 0\}$. The Fourier transform consists then of N complex values $\{\mathbb{S}_{k0}, \mathbb{S}_{k1}, \ldots, \mathbb{S}_{kN-1}\}$. The real parts, $\{R_{k0}, R_{k1}, \ldots, R_{kN-1}\}$, are retained only and are stored back in place of the original FID. After transformation of all FID's, the matrix $\{R_{kj}\}$ is transposed, $\{R_{kj}\} \rightarrow \{R_{jk}\}$, and each row, augmented by N zero values, is Fourier-transformed a second time. The absolute values of the N^2 complex Fourier coefficients are then utilized for the plot of a two-dimensional zeugmatogram. It can easily be shown that the neglect of the imaginary part after the first Fourier transformation does not cause any loss of information nor does it deteriorate the sensitivity.

The limited number of samples available to represent each FID calls for a careful selection of the center frequency, of the strength of the applied field gradients and of the sampling rate, such that the spatial resolution is sufficient without violating the sampling theorem and avoiding frequency foldover which can seriously distort a zeugmatogram. It must be remembered that dispersion-like parts as well must be represented. Dispersion mode signals have a much higher tendency to cause problems with frequency foldover than absorption mode signals because of the much broader wings of the former.

The number of samples N has been selected to be 64. This results in a total of 4096 sample values. The time required for one complete experiment including the data transformation is 8 min and the plotting of the 64×64 zeugmatogram on the teletype requires another 7 min.

The NMR samples that were used to demonstrate the principle of Fourier zeugmatography consisted of two parallel glass capillary tubes filled with H_2O. For Figs. 3 and 4, the two capillaries, with an inner diameter of 1.0 mm and a separation of the centers by 2.2 mm, were surrounded with D_2O. The sample was positioned in the magnet gap such that the capillary tubes were parallel to the y-axis and the line joining the centers of the two tubes was parallel to the z-axis. Figure 3 shows a series of typical FID's and their first Fourier transform. During the first time-interval of length t_x, a linear gradient of 500 Hz/cm was applied along the x-axis. The two capillary tubes are then in the same local field and the FID remains unmodulated as is demonstrated by Fig. 3. During the second time-interval, a gradient of 700 Hz/cm was applied along the z-axis. It causes the two tubes to be in different local fields and it is responsible for the modulation of the FID as well as for the doublet structure of the first Fourier transform with respect to t_z, shown on the right-hand side of Fig. 3. The phase and amplitude of the signal after the first Fourier transformation map out the FID at the end of the first time-interval. A

FIG. 3. Nine typical FID's selected out of a complete set of 64 signals obtained for pulsed linear field gradients along the x- and z-axis. The corresponding Fourier transforms are shown on the right-hand side. The numbers on the ordinate represent the time intervals in terms of sampling cycles during which the x-gradient was on. The broken vertical lines in the FID's indicate the point in time when the x-gradient was stopped and the z-gradient was switched on. At the same time, the recording of the FID was started. The sample consisted of two parallel capillary tubes arranged such that their centers were lying on the z-axis. The sampling interval was 0.5 msec giving a total spectral width of 1 kHz.

second Fourier transformation with respect to t_x then yields the final two-dimensional Fourier zeugmatogram shown in Fig. 4. For this map, the total intensity range has been divided into eight equal intervals and a teletype character assigned to each interval. The intensity intervals are indicated in increasing order by the symbols (blank), •, *, A, B, C, D, and E, respectively. This assignment is used for all zeugmatograms given in this paper.

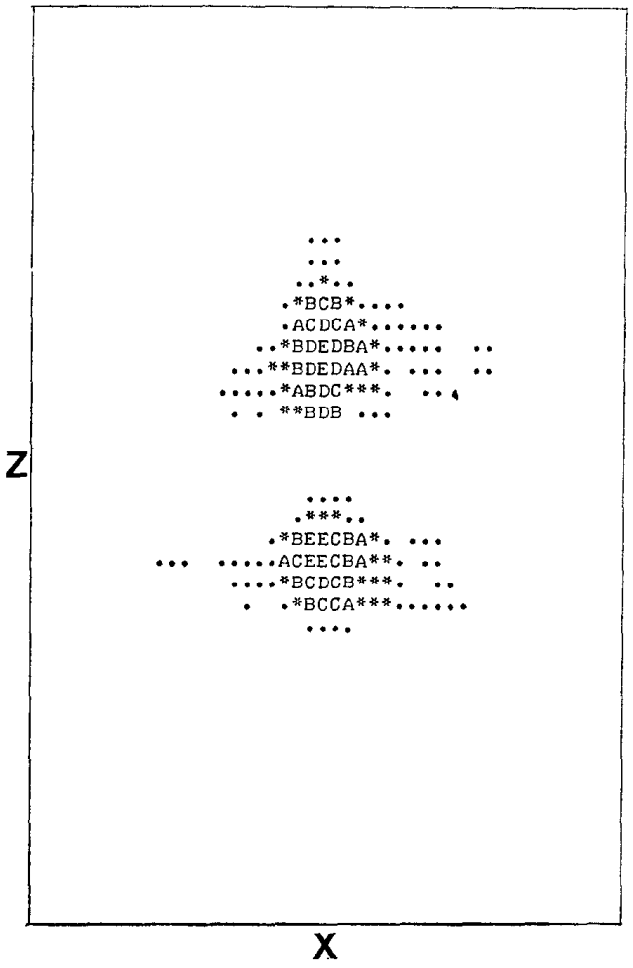

FIG. 4. The Fourier zeugmatogram obtained from the data partially shown in Fig. 3. The absolute value $|\bar{c}(r')|$ of the spin density function is plotted as a function of x and z. Only the central section of the 64 × 64 zeugmatogram is shown.

Figures 5 and 6 show a series of FID signals along with their first Fourier transforms and the Fourier zeugmatogram computed therefrom for the same experimental parameters and for the same sample as used for Figs. 3 and 4, except that the two gradients have been interchanged in time. The first gradient is now along the z-axis and the second along the x-axis. In this case, phase and amplitude of the first Fourier transform clearly show the beats caused by the different local fields of the two capillaries during the first time interval. Figures 4 and 6 represent images of the same sample effectively rotated by 90°. The two zeugmatograms do not exactly match due to experimental imperfections which will be discussed below.

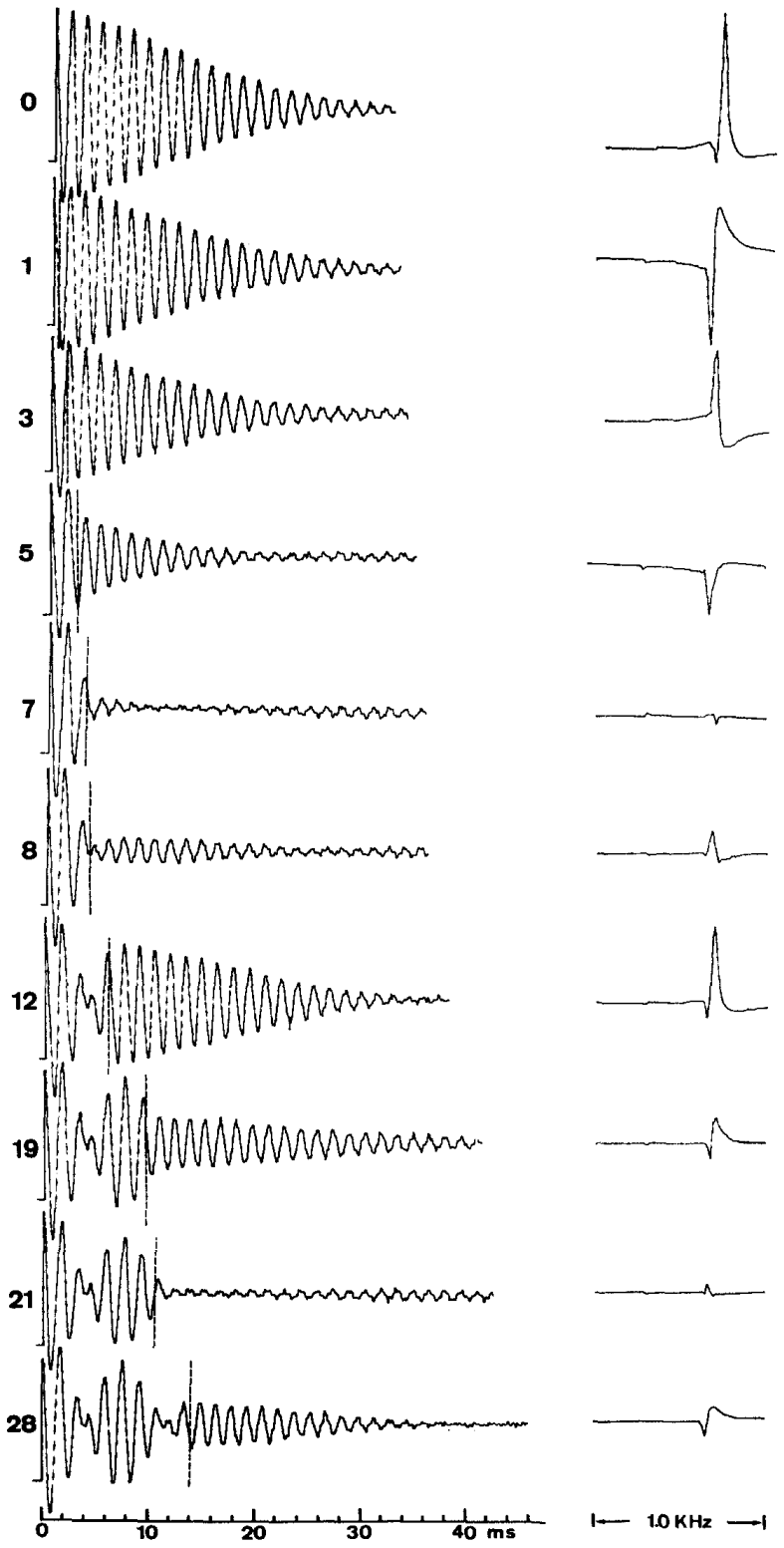

FIG. 5. Ten typical FID signals and their Fourier transforms obtained for the same conditions as in Fig. 3, but with the x- and z-gradients interchanged in time. The FID is recorded in this case during the time the x-gradient is on.

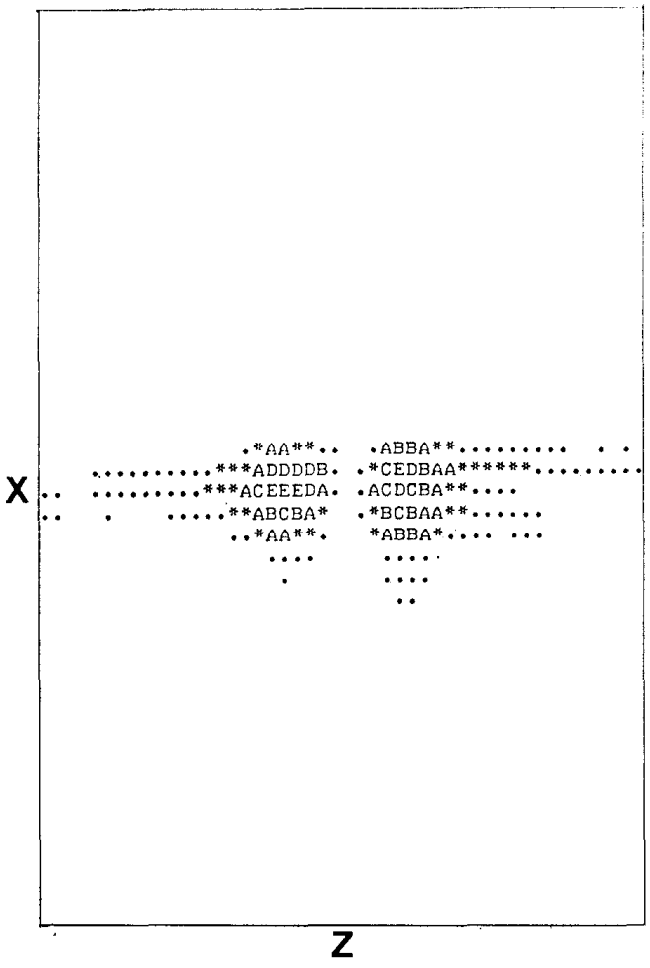

FIG. 6. The Fourier zeugmatogram calculated from the data partially shown in Fig. 5. The x- and z-axis are interchanged as compared to Fig. 4. Only the central section of the 64 × 64 zeugmatogram is shown.

Figure 7 gives the zeugmatogram of another sample consisting of two capillary tubes, with an inner diameter of 1.3 mm and a separation of the centers of 2.6 mm, placed in the magnet gap such that the line joining the centers was making an angle of about 30° to the z-axis. This sample had no D_2O outside the capillaries and the change in susceptibility required a retuning of the basic magnetic field homogeneity. This figure demonstrates the two-dimensional resolution of Fourier zeugmatography.

The zeugmatograms shown in this paper were obtained mainly to demonstrate the principle of the technique and therefore a very simple sample geometry was used. With future applications in view, it may be worthwhile to point out some of the problems that were encountered. These problems are most likely responsible for some of the spread and for the limited resolution of the zeugmatograms shown. We believe that it is possible to improve the images by paying attention to the following points.

(*a*) *Linearity and homogeneity of the gradients.* It is obvious that in any zeugmatographic technique the linearity and the homogeneity of the applied field gradients is of crucial importance. Very often, the shim coils provided in commercial spectrometer

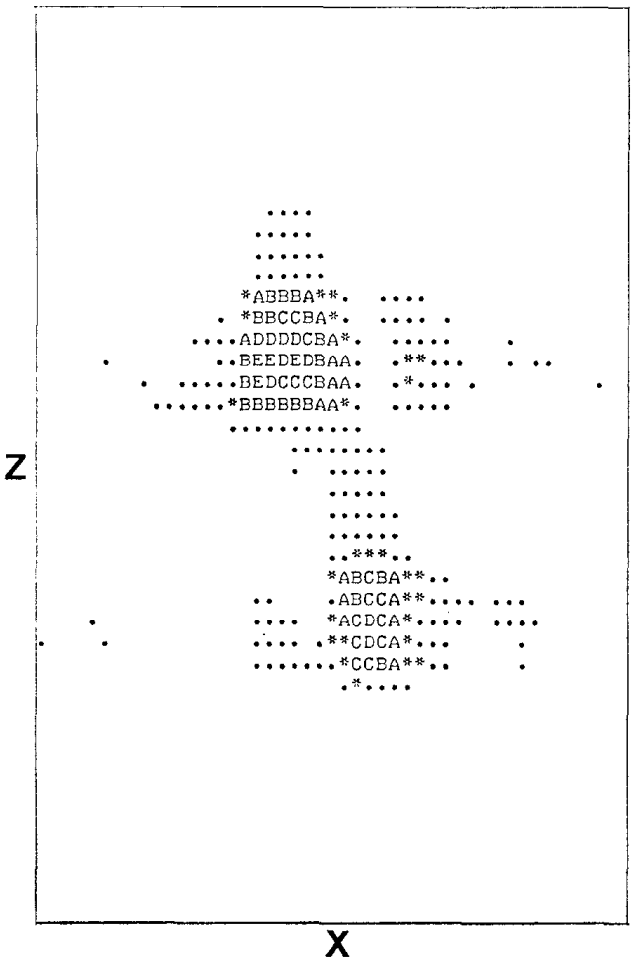

FIG. 7. Fourier zeugmatogram of a sample consisting of two parallel capillaries with their centers lying on a line making an angle of about 30° to the z-axis. The first x-gradient was 600 Hz/cm and the second z-gradient was 700 Hz/cm. The absolute value $|\bar{c}(r')|$ of the spin density function is plotted as a function of x and z. Only central section of the 64 × 64 zeugmatogram is shown.

systems produce gradients that are not of sufficient linearity over the entire sample volume. It may, therefore, be advisable to add special gradient coils with improved linearity (*10*).

(*b*) *Rise and fall time of the gradients.* The described pulsed version of zeugmatography relies on the instantaneous application and removal of field gradients. Eddy currents in pole caps and metal shields can cause response-time problems that will result in serious distortions of the zeugmatogram. Special arrangements of gradient coils which minimize the rise and fall time of the gradients have been described by Tanner (*10*).

(*c*) *Susceptibility problems.* In many samples, the local magnetic field is already inhomogenous due to variations of the susceptibility and due to the particular shape of the sample. It is then necessary to apply sufficiently strong gradients to overcome these "natural" field gradients.

The pictorial representation could certainly be improved for visual effects by more sophisticated means, for example, by means of a computer-controlled display.

IV. EXTENSIONS OF THE TECHNIQUE

Many possible extensions of the described technique exist. They have not yet been pursued in great detail. This section gives a brief description of some of the possibilities.

(*a*) *Recording of a Pure Absorption Mode Zeugmatogram*

It may be desirable to completely separate absortion- and dispersion-like parts as the absorption mode signal has an inherently higher resolution than the absolute value signal. The pure absorption mode may often produce a more accurate zeugmatogram. This separation can be achieved by the following modification of the basic technique. For each set of values t_x and t_y, a series of four different experiments is performed and the four resulting FID's are averaged:

$$s_{\mathrm{av}}(\mathbf{t}) = \tfrac{1}{4}\{s^{+++}(\mathbf{t}) + s^{++-}(\mathbf{t}) + s^{+-+}(\mathbf{t}) + s^{-++}(\mathbf{t})\}. \qquad [13]$$

The four experiments differ by the signs of the applied field gradients and by the position of the reference frequency ω_1 above or below resonance (negative or positive frequency offset Δ). The notation of Eq. [13] is explained in Table 1. For this technique, it is not only necessary to switch gradients between the three phases of the FID but also to

TABLE 1

GRADIENTS AND RESONANCE OFFSETS IN THE FOUR REQUIRED EXPERIMENTS

	Applied gradients η			Resonance offset Δ		
Time interval	t_x	t_y	t_z	t_x	t_y	t_z
$s^{+++}(\mathbf{t})$	η_x	η_y	η_z	$\lvert\Delta\rvert$	$\lvert\Delta\rvert$	$\lvert\Delta\rvert$
$s^{++-}(\mathbf{t})$	η_x	η_y	$-\eta_z$	$\lvert\Delta\rvert$	$\lvert\Delta\rvert$	$-\lvert\Delta\rvert$
$s^{+-+}(\mathbf{t})$	η_x	$-\eta_y$	η_z	$\lvert\Delta\rvert$	$-\lvert\Delta\rvert$	$\lvert\Delta\rvert$
$s^{-++}(\mathbf{t})$	$-\eta_x$	η_y	η_z	$-\lvert\Delta\rvert$	$\lvert\Delta\rvert$	$\lvert\Delta\rvert$

change the sign of the resonance offset Δ. This can be achieved by an appropriate change of the dc magnetic field (during the off-time of the field-frequency lock) or, better, by a sudden change of the reference frequency of the phase-sensitive detector, ω_1. Care must be taken to retain phase coherence during this frequency switching.

By means of Eq. [3] and utilizing the trigonometric addition theorems, one obtains for $s_{\mathrm{av}}(\mathbf{r},\mathbf{t})$

$$s_{\mathrm{av}}(\mathbf{r},\mathbf{t}) = M_0 \cos((\Delta + \eta_x x)\, t_x) \cos((\Delta + \eta_y y)\, t_y) \cos((\Delta + \eta_z z)\, t_z) \cdot \exp\{-(t_x + t_y + t_z)/T_2\}. \qquad (14)$$

In this expression, the three variables t_x, t_y, and t_z are separated. The three-dimensional Fourier transformation is now executed step-by-step, and, after each transformation, the imaginary part is eliminated. This is equivalent to a three-dimensional cosine transformation and gives the result

$$S_{\mathrm{av}}(\omega) = \iiint c(\mathbf{r})\, S_{\mathrm{av}}(\mathbf{r},\omega)\, dv \qquad (15)$$

with

$$S_{av}(\mathbf{r},\omega) = \tfrac{1}{8}\{A(\Delta + \eta_x x - \omega_x) + A(-\Delta - \eta_x x - \omega_x)\} \cdot \{A(\Delta + \eta_y y - \omega_y) + A(-\Delta - \eta_y y - \omega_y)\} \cdot \{A(\Delta + \eta_z z - \omega_z) + A(-\Delta - \eta_z z - \omega_z)\}. \quad [16]$$

This is a three-dimensional absorption mode signal and is the desired result. The contribution of the negative resonances can again be neglected, in general, and the function is converted into a function of $\mathbf{r}'$, $\bar{c}_{av}(\mathbf{r}') = S_{av}(\omega)$, in analogy to Eqs. [11] and [12], and plotted as a function of x, y and z.

In two dimensions, a series of only two experiments is necessary to determine $s_{av}(\mathbf{t})$:

$$s_{av}(\mathbf{t}) = \tfrac{1}{2}\{s^{++}(\mathbf{t}) + s^{+-}(\mathbf{t})\}. \quad [17]$$

It is obvious that this modified technique is more complicated. It has not yet been used, and it is not clear in which cases it is worth the effort.

(b) Recording of a Two-Dimensional Cross Section

It has been mentioned that a full three-dimensional zeugmatogram requires an amount of data that goes beyond the capacity of most small computers. The two-dimensional mapping described in Section III, on the other hand, does not provide distinct cross sections but rather a projection of the three-dimensional spin density onto a two-dimensional plane. In many circumstances, a true cross section would be more desirable.

A cross section can be obtained by the following technique. A quadratic or possibly higher order gradient is applied along the third direction, e.g., the y-axis. Then, only the volume elements near $y = 0$ will appreciably contribute to the signal amplitude. The remaining contributions will be smeared over a much larger spectral region and may be disregarded. For an additional smearing, it is also possible to average several FID's for various field gradients along the y-axis. For the selection of another cross section perpendicular to the y-axis, the sample has to be moved along the y-axis.

A limited confinement to a cross-sectional area is also possible by using very short receiver and transmitter coils.

(c) Improved Resolution with Limited Core Memory

An improved representation of a zeugmatogram may be obtained in the following way when the memory space is limited. Each FID is sampled to obtain M sample values which are Fourier-transformed to produce a spectrum containing M samples. The sampling rate may be selected such that the interesting part of the spectrum covers only a small portion of the total spectrum. N significant, not necessarily equally spaced, samples of the spectrum are selected and stored for the subsequent second Fourier transformation. The number of relevant samples, N, can be considerably smaller than M. All other sample values can be discarded to save memory space. A similar procedure for the second Fourier transform is unfortunately not possible.

(d) Measurement of Relaxation Times

The measurement of the two- or three-dimensional distribution of spin–lattice relaxation times can be achieved by straightforward extensions of the inversion-recovery technique (*11*) or of the saturation recovery method (*12*). The spin system is prepared

at $t = -T$ by means of a 180° pulse or by means of a saturating burst of rf pulses. The zeugmatogram obtained with a 90° pulse at $t = 0$ is then a measure for the spatial dependence of the recovery of the z-magnetization during the time T and permits determination of $T_1(\mathbf{r})$. An adaptation of the progressive saturation technique (*13*) is also feasible.

(*e*) *Related Techniques*

A somewhat related technique has been described by Mansfield and Grannell (*14*). It is called NMR diffraction and its aim is the determination of the periodic structure of a solid by applying a single linear field gradient and recording the FID signal under high resolution conditions. This technique could also be generalized by applying a sequence of pulsed field gradients in the same manner as described in the present paper.

Two further techniques which also involve time-dependent magnetic field gradients have recently been described by Hinshaw (*15*). Of particular interest seems to be his "sensitive point method" as it permits picking out the signals originating from a distinct point within a three-dimensional object.

It should also be mentioned that the technique of Fourier zeugmatography is remotely related to pulse-pair Fourier spectroscopy as proposed by Jeener (*16*). In this technique, which has a completely different aim, two 90° rf pulses are applied at $t = 0$ and at $t = t_1$. The free induction decay signal after the second pulse is then a function of the two time parameters t_1 and $t_2 = \mathrm{t} - \mathrm{t}_1$, $s(t_1, t_2)$. It resembles the signal obtained in two-dimensional Fourier zeugmatography. Its two-dimensional Fourier transform produces a two-dimensional spectrum that contains information of the kind usually obtained in double resonance experiments. It does not give information about the spatial distribution of nuclear spins. But the same experimental set-up and particularly the same computer programs can be used for both techniques.

More sophisticated extensions are conceivable, like the measurement of the spatial distribution of flow by measuring the echo height in a spin–echo experiment in an inhomogenous magnetic field. Various double resonance techniques can also be combined with zeugmatography, for example, to single out the contributions of one particular resonance line in a more complex spin system. Fourier zeugmatography has the potential to adopt many of the well-known pulse techniques presently in use in high resolution NMR of liquids and of solids.

ACKNOWLEDGMENTS

This work has partially been supported by the Swiss National Foundation of Science. The receipt of a preliminary manuscript by J. Jeener and G. Alewaeters is gratefully acknowledged. A discussion with P. Lauterbur has considerably helped to clarify several points.

REFERENCES

1. P. C. Lauterbur, *Nature (London)* **242,** 190 (1973).
2. R. Damadian, *Science* **171,** 1151 (1971).
3. I. D. Weisman, L. H. Bennett, L. R. Maxwell, M. W. Woods, and D. Burk, *Science* **178,** 1288 (1972).
4. D. J. De Rosier and A. Klug, *Nature (London)* **217,** 130 (1968).
5. R. Gordon and G. T. Herman, *Comm. ACM* **14,** 759 (1971).
6. G. T. Herman, A. Lent, and S. W. Rowland, *J. Theor. Biol.* **42,** 1 (1973).

7. A. KLUG AND R. A. CROWTHER, *Nature (London)* **238,** 435 (1972).
8. R. R. ERNST AND W. A. ANDERSON, *Rev. Sci. Instr.* **37,** 93 (1966).
9. E. BARTHOLDI AND R. R. ERNST, *J. Magn. Resonance* **11,** 9 (1973).
10. J. E. TANNER, *Rev. Sci. Instr.* **36,** 1086 (1965).
11. R. L. VOLD, J. S. WAUGH, M. P. KLEIN, AND D. E. PHELPS, *J. Chem. Phys.* **48,** 3831 (1968).
12. J. L. MARKLEY, W. J. HORSLEY, AND M. P. KLEIN, *J. Chem. Phys.* **55,** 3604 (1971); W. A. ANDERSON, R. FREEMAN, AND H. HILL, *Pure Appl. Chem.* **32,** 27 (1972).
13. R. FREEMAN AND H. D. W. HILL, *J. Chem. Phys.* **54,** 3367 (1971).
14. P. MANSFIELD AND P. K. GRANNELL, *J. Phys. C Solid State Phys.* **6,** L422 (1973).
15. W. S. HINSHAW, *Phys. Lett.* **48A,** 87 (1974).
16. J. JEENER AND G. ALEWAETERS, private communication (1973).